Using finite element modelling and experimental methods to investigate planar coil sensor topologies for inductive measurement of displacement

Gregory Moreton, Turgut Meydan, and Paul Williams

Citation: AIP Advances **8**, 047503 (2018); doi: 10.1063/1.4994127
View online: https://doi.org/10.1063/1.4994127
View Table of Contents: http://aip.scitation.org/toc/adv/8/4
Published by the American Institute of Physics

Using finite element modelling and experimental methods to investigate planar coil sensor topologies for inductive measurement of displacement

Gregory Moreton, Turgut Meydan,[a] and Paul Williams
Wolfson Centre for Magnetics, School of Engineering, Cardiff University, Cardiff CF24 3AA, United Kingdom

(Received 4 July 2017; accepted 26 August 2017; published online 16 October 2017)

The usage of planar sensors is widespread due to their non-contact nature and small size profiles, however only a few basic design types are generally considered. In order to develop planar coil designs we have performed extensive finite element modelling (FEM) and experimentation to understand the performance of different planar sensor topologies when used in inductive sensing. We have applied this approach to develop a novel displacement sensor. Models of different topologies with varying pitch values have been analysed using the ANSYS Maxwell FEM package, furthermore the models incorporated a movable soft magnetic amorphous ribbon element. The different models used in the FEM were then constructed and experimentally tested with topologies that included mesh, meander, square coil, and circular coil configurations. The sensors were used to detect the displacement of the amorphous ribbon. A LabView program controlled both the displacement stage and the impedance analyser, the latter capturing the varying inductance values with ribbon displacement. There was good correlation between the FEM models and the experimental data confirming that the methodology described here offers an effective way for developing planar coil based sensors with improved performance. https://doi.org/10.1063/1.4994127

I. INTRODUCTION

Recently, there has been renewed interest in planar coil technology due to its potential for sensing in nondestructive evaluation (NDE) applications and for wireless power transmission.[1–4] The advantages of planar coils over traditional wound coils include small size profile,[5,6] wireless sensing capabilities,[7,8] and low cost and greater robustness.[9,10] They can also be manufactured on flexible or hard substrates depending on the application.[11–13] Planar coil inductance is influenced by both physical or electromagnetic factors[8,14–17] and are often implemented as part of an LC circuit, where changes to the inductance value affects the resonance of the LC circuit.[11] These characteristics allow for many potential applications such as health monitoring,[7,18] NDT, NDE,[10,19–23] wireless power transfer,[3,13] and sensing.[24–27]

Geometry plays an important role in the performance of planar coils leading to changes in the resistance, inductance, quality factor, and resonant frequency of the coil.[5,28–31] Numerical descriptions of various type of planar coil have been reported[3,5,32] however there is still much scope to model their behaviour in sensing applications.

In this work we investigated the behaviour of various planar coil structures as part of a displacement sensor. Four different coil topologies (square, circular, meander and mesh) with varying pitch values were evaluated using the ANSYS Maxwell 3D FEM package. Manufactured versions were then characterized using an impedance analyser. This work presents a comparison of both simulated and measured performance of each displacement sensor design.

[a]E-mail: Meydan@cardiff.ac.uk

II. SENSOR DESIGN AND MODELLING

Each sensor is a composite design combining a planar coil with a 25 mm wide amorphous ribbon element. This constrained the dimensions of the sensor to 25 mm x 25 mm. It was necessary to model the planar coils in three dimensions, due to the asymmetry of the meander and mesh coil topologies and the geometrical arrangement of the coil relative to the ribbon element. Table I lists the pitch values and Fig. 1 shows illustrations of the four topologies used in this study. The square and circular coil topologies represent spiral coil designs, where the coil expands outwards in a spiral pattern. Additional spiral coil topologies were omitted for simplification due to the large amount of variation. The meander and mesh coil topologies are non-spiral designs which have been chosen to compare against spiral coil designs. These coils have been selected due to them being more prevalently used in planar sensor design and relative ease of fabrication, along with good physical and magnetic coupling with the magnetic ribbon element used in the sensor. Three pitch values were chosen for each topology, resulting in 12 planar coil configurations. A boundary of 40 mm x 40 mm x 20 mm was applied to the models based on a preliminary investigation showing that the operating range of the square planar coil was around 10 mm. Pitch values were chosen to conform with the area constraint and populate the area efficiently. Due to the limitation of the fabrication method, described in III, the pitch values chosen for the mesh topology are larger than those for the other coil types.

Inductance changes were modelled using material parameters based on a Metglas 2605S3A amorphous ribbon i.e. 25 mm x 25 mm, 18 μm thickness, and relative permeability of 20000. Inductance as a function of distance between the ribbon and the planar coil was modelled using a parametric sweep. The ribbon was displaced 10 mm in total using a decade sweep with 10 steps per

TABLE I. List of topologies and respective pitch values.

Topology	Pitch 1 (mm)	Pitch 2 (mm)	Pitch 3 (mm)
Circular Coil	0.5	0.75	1.0
Square Coil	0.5	0.75	1.0
Meander Coil	0.5	0.75	1.0
Mesh Coil	1.0	2.5	3.5

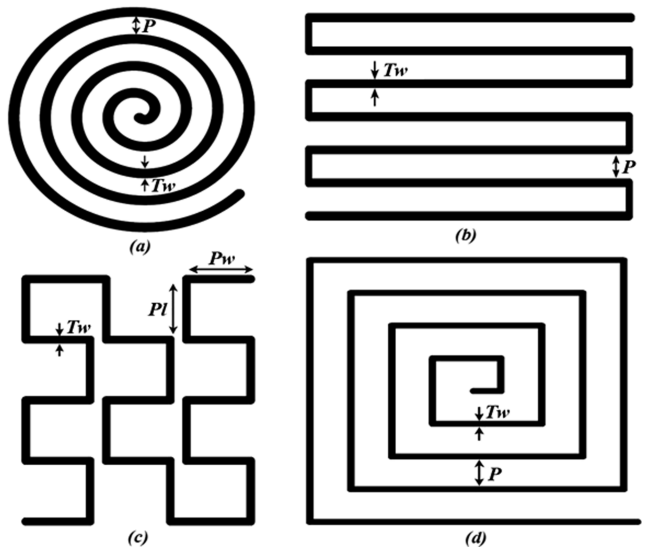

FIG. 1. Examples of coil topologies, with *P* being the pitch and *Tw* being the track width. (a) The circular coil topology. (b) The meander coil topology. (c) The mesh coil topology, with *Pw* representing the width of each mesh segment and *Pl* representing the length of each mesh segment, for simplification *Pw* and *Pl* have been designed to be equal in all mesh coils. (d) The square coil topology.

decade. This was sufficient to model sensor performance for later comparison with experimental data. A percentage error of 2% was applied to all of the simulations.

III. SENSOR FABRICATION AND EXPERIMENTAL DETAILS

The planar coils shown in Fig. 2 were milled from a 54 mm x 30 mm FR4 PC board (35μm copper thickness) using a track width of 0.5 mm and track gaps were varied according to the desired pitch value. A number of 3D printed polymer supports, shown in Fig .3, were used to secure the planar coil and amorphous ribbon to separate displacement stages. The measurement involved displacement of the Metglas 2605S3A amorphous ribbon relative to the stationary coil under the control of a LabVIEW program interfaced to a KDC101 DC servo motor controller as shown in Fig. 4. In this case the ribbon was as cast (i.e. no annealing treatments) with a thickness of 18 μm, a relative permeability of 20000 and dimensions of 25.4 mm x 30 mm. Due to the need to attach the ribbon to the support structure, the ribbon is longer than the modelled sample.

The planar coil was characterized using the Agilent 4294A impedance analyser and 16089B Kelvin clip attachment with a frequency range limited to 5 Hz – 100 kHz. The impedance analyser collected inductance data for each displacement step of the coil starting at 0 mm with respect to the coil and finishing at 10 mm. Step size was set to 200 μm and measurements over the whole displacement range were repeated ten times for each coil.

IV. DISCUSSION

The FEM displacement results in Fig. 5 show the largest inductance value for the square coil, followed by the circular, meander and mesh coil. There are two distinct characteristics here, one for the square and circular coils and another for the meander and mesh coils. The meander coil has

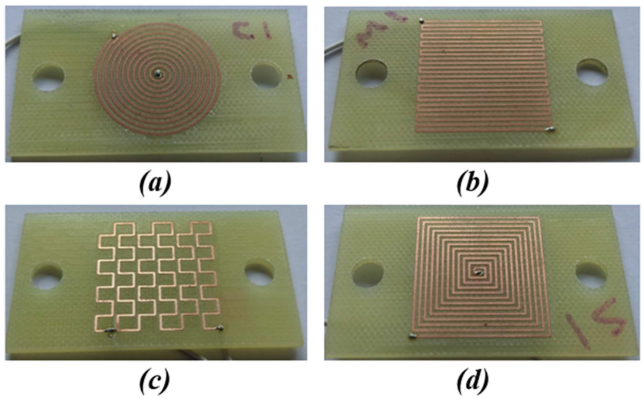

FIG. 2. Examples of fabricated coils on PCB, with holes for 3D printed support structures. (a) Circular coil topology. (b) Meander coil topology. (c) Mesh coil topology. (d) Square coil topology.

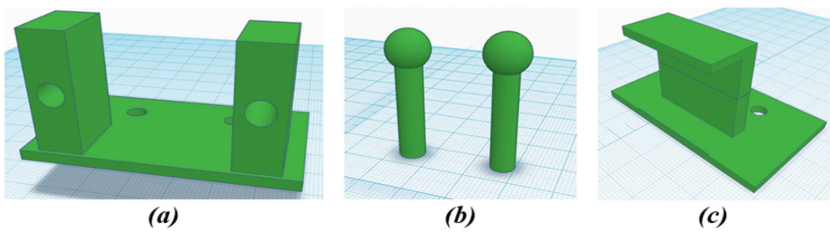

FIG. 3. 3D models of supporting structures. (a) Planar coil holder. (b) Holder pins, for inserting through holes of planar coil PCB to secure it to the holder. (c) Magnetic ribbon holder.

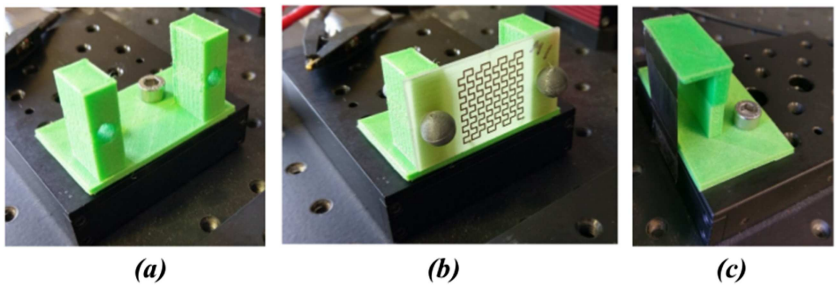

FIG. 4. Printed 3D structures secured on displacement stage. (a) Planar coil holder with no coil attached. (b) Planar coil holder with mesh coil attached. (c) Magnetic ribbon holder with ribbon attached.

the lowest measurement range, of approximately 2.5 mm, and the circular and square coils have the largest range equal to approximately 10 mm. The meander coil with the pitch of 0.5 mm has the lowest measurement range, followed by the mesh coil with the pitch of 1 mm. These pitch values are the lowest for each topology, respectively. In contrast the square and circular coil topologies with the lowest pitch value, of 0.5 mm, demonstrate good measurement range compared to coils of the same topology but with larger pitch values.

The simulation results demonstrate that changes to the coil topology enable the sensitivity to match the desired displacement range. The pitch values chosen in this work clearly affect the inductance but do not significantly influence the shape of the signal-displacement profile. For the square and circular coil topologies, a reduction in pitch increases the number of turns and therefore the inductance as expected. This relationship is not as obvious for the meander and mesh designs but similar increases in inductance are also observed. This could be due to the effect of mutual inductance, as the interaction between the copper tracks increases as the area becomes more densely populated. It can be seen that the inductance changes are proportional to the planar coil's self-inductance, therefore this value should be maximized to optimize displacement sensitivity.

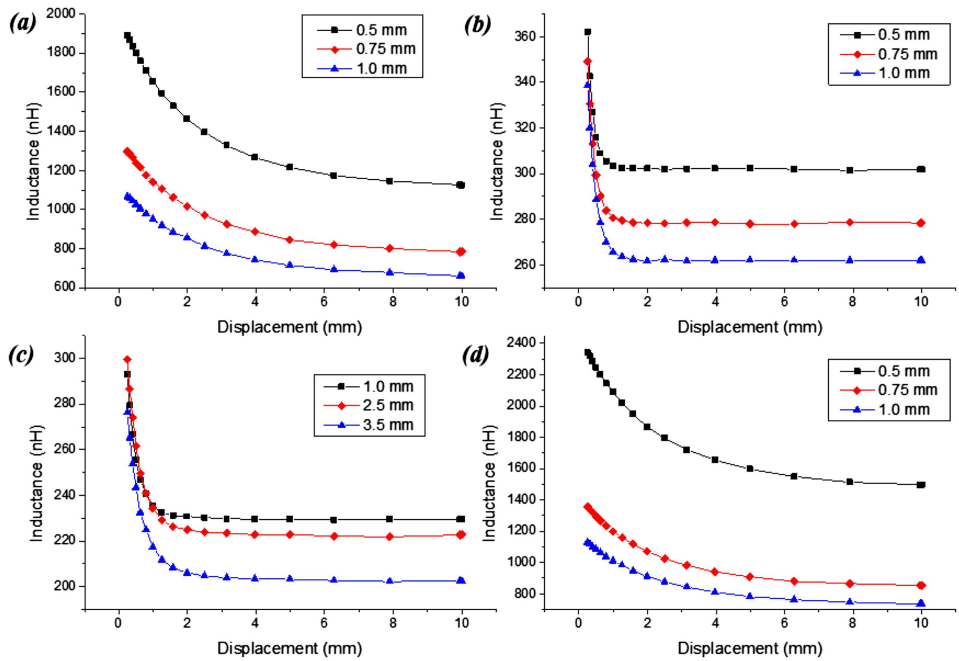

FIG. 5. 3D FEM results of displacement simulation with varying pitches. (a) Circular coil topology. (b) Meander coil topology. (c) Mesh coil topology. (d) Square coil topology.

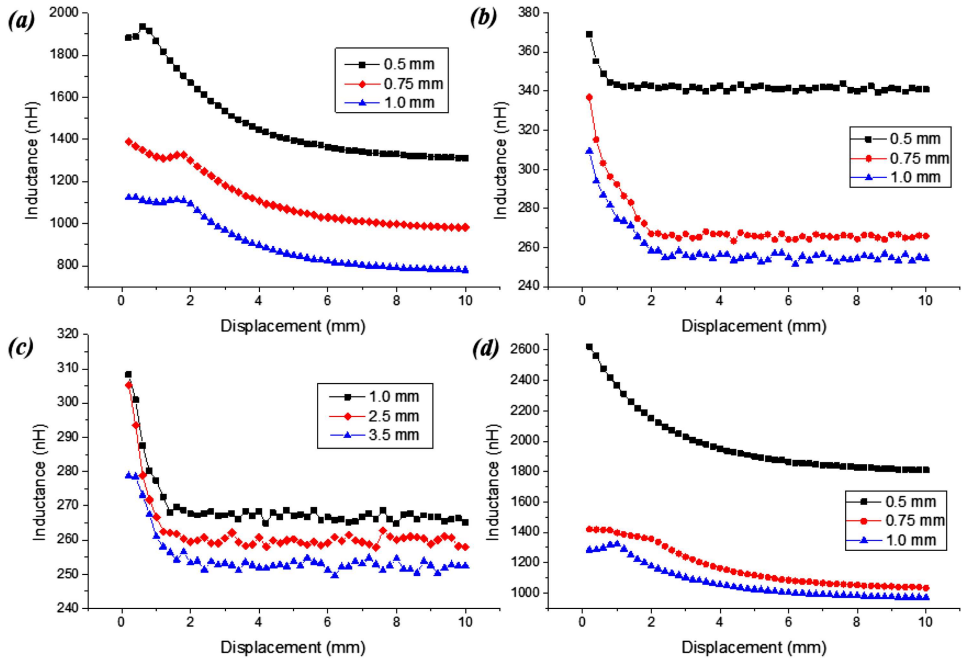

FIG. 6. Experimental results of displacement investigation of planar coils with varying pitches. (a) Circular coil topology. (b) Meander coil topology. (c) Mesh coil topology. (d) Square coil topology.

The experimental results obtained from actual displacement measurements are shown in Fig. 6. It can be seen that the fabricated coils follow similar trends to their FEM counterparts in Fig. 5, most notably the maximum distance for detection. All of the fabricated coils have a larger inductance than the simulated values, with the square and circular coil topologies nearly doubling in inductance. Signal irregularities are present in both the circular and square coils and are most prominent at larger pitch values, however the correlation between these coils and the simulations are otherwise good. These irregularities did not appear in the mesh or meander topologies. The data presented is the inductance value at 80 kHz, and is representative of the range from 20 kHz – 100 kHz. Data below 20 kHz had a small signal to noise ratio. Calculating the standard deviation of each data point over ten measurements, gave an error of ±3.5 nH, the error bars have been omitted from Fig. 6 for clarity. The main source of this error comes from the impedance analyser.

To further analyse sensor performance both FEM and experiment data were fitted with an exponential decay trend line. The exponential decay fit was in good agreement with the data, with r^2 values ranging from 0.99 to 0.95. The decay constant for the mesh and meander topology is much larger than the square and circular coils, resulting in a more rapid inductance decrease. The sensitivity of the sensor is difficult to quantify due to the nonlinear nature of the sensor. However, by using a linear fit over a limited range, an approximate sensitivity has been calculated in Table II.

It can be seen that the spiral coil topologies have a much larger operating range in a displacement sensing application, a larger inductance value, and greater sensitivity. These parameters increase proportionately with decreasing pitch dimension. These results indicate that for inductive sensing of displacement, planar coils should employ spiral coil topologies, preferably square, with the highest

TABLE II. List of topologies and approximate sensitivities.

Topology	Pitch 1 (nH/mm)	Pitch 2 (nH/mm)	Pitch 3 (nH/mm)
Circular Coil	122 (up to 5 mm)	72 (up to 5 mm)	67 (up to 5 mm)
Square Coil	140 (up to 5 mm)	73 (up to 5 mm)	68 (up to 5 mm)
Meander Coil	27 (up to 1 mm)	34 (up to 2 mm)	25 (up to 2 mm)
Mesh Coil	21 (up to 2 mm)	23 (up to 2 mm)	16 (up to 2 mm)

copper track density for the best sensor performance. However, design considerations depend very much on the application and it is difficult to apply general design rules other than that mentioned above.

V. CONCLUSION

This paper has presented an investigation into the use of various planar coil topologies for displacement sensing. The work has compared FEM simulation with experimental measurements showing good correlation between the two. We have demonstrated that coil topology significantly affects sensor performance thus enabling optimization of sensor sensitivity and displacement range. Coils based on a mesh or meander pattern were found to have significantly less range of operation compared to the square and circular coil configurations. In general, experimental measurements were consistent with FEM predictions, however some anomalies at small displacements with the square and circular coils, suggests that some of the assumptions made in the FEM model requires further scrutiny. In future work we plan to refine our modelling approach and to investigate other soft magnetic materials as part of the inductive element.

ACKNOWLEDGMENTS

The authors would like to thank the Engineering and Physical Sciences Research Council for its support through a Doctoral Training Grant (Ref EP/M50631X/1), without which this research would not have been possible.

[1] S. Mukhopadhyay, IEEE Sensors Journal **4**, 301 (2004).
[2] S. Yamada, M. Katou, M. Iwahara, and F. Dawson, IEEE Transactions On Magnetics **31**, 3185 (1995).
[3] B. H. Waters, B. J. Mahoney, G. Lee, and J. R. Smith in *2014 IEEE International Symposium on Circuits and Systems (ISCAS)*, Melbourne, 2014, pp. 2045–2048.
[4] K. Hao, S. Huang, W. Zhao, S. Wang, and J. Dong, NDT & E International **44**, 274 (2011).
[5] U. Jow and M. Ghovanloo, IEEE Transactions On Biomedical Circuits And Systems **1**, 339 (2007).
[6] L. Dong, L. F. Wang, Q. Y. Ren, and Q. A. Huang, in *IEEE SENSORS 2014 Proceedings*, Valencia 926–929 (2014).
[7] G. Chen, I. Chan, L. Leung, and D. Lam, Medical Engineering & Physics **36**, 1134 (2014).
[8] M. A. Fonseca, M. G. Allen, J. Kroh, and J. White in *Solid-State Sensor, Actuator, and Microsystems Workshop*, South Carolina, 2006, pp. 37–41.
[9] S. Ali, A. Hassan, J. Bae, C. Lee, and J. Kim, Langmuir **32**, 11432 (2016).
[10] S. Mukhopadhyay, C. Gooneratne, G. S. Gupta, and S. Demidenko, IEEE Transactions On Instrumentation And Measurement **55**, 1331 (2006).
[11] G. Moreton, T. Meydan, and P. Williams, IEEE Transactions On Magnetics **52** (2016).
[12] C. Yang, J. Chien, B. Wang, P. Chen, and D. Lee, Biomedical Microdevices **10**, 47 (2007).
[13] F. Jolani, Y. Yu, and Z. Chen, IEEE Antennas And Wireless Propagation Letters **13**, 1648 (2014).
[14] Q. A. Huang, L. Dong, and L. F. Wang, Journal of Microelectromechanical Systems **25**, 822 (2016).
[15] R. Nopper, R. Niekrawietz, and L. Reindl, IEEE Transactions on Instrumentation and Measurement **59**, 2450 (2010).
[16] R. Ditchburn and S. Burke, NDT & E International **38**, 690 (2005).
[17] J. Fava, L. Lanzani, and M. Ruch, NDT & E International **42**, 713 (2009).
[18] S. Yoon, J. K. Sim, and Y. H. Cho in *IEEE SENSORS 2014 Proceedings*, Valencia, 2014, pp. 851–854.
[19] S. Mukhopadhyay, IEE Proceedings - Science, Measurement And Technology **149**, 165 (2002).
[20] S. Mukhopadhyay and C. Gooneratne, IEEE Sensors Journal **7**, 1340 (2007).
[21] J. Fava and M. Ruch, Insight - Non-Destructive Testing And Condition Monitoring **46**, 268 (2004).
[22] A. Mohd Syaifudin, K. Jayasundera, and S. Mukhopadhyay, Sensors And Actuators B: Chemical **137** (2009).
[23] P. Tse, X. Liu, Z. Liu, B. Wu, C. He, and X. Wang, Smart Materials And Structures **20**, 055001 (2011).
[24] H. Chang, S. Liao, H. Hsieh, J. Wen, C. Lai, and W. Fang, Sensors And Actuators A: Physical **238**, 25 (2016).
[25] S. Djuric, IEEE Transactions On Magnetics **50** (2014).
[26] H. C. Chang, S. C. Liao, H. S. Hsieh, S. Lin, C. H. Lai, R. Chen, and W. Fang in *Proceedings of the IEEE International Conference on Micro Electro Mechanical Systems (MEMS)*, Taipei, 2013, pp. 685–688.
[27] S. Sauer and W. Fischer, Procedia Engineering **47**, 750 (2012).
[28] Y. Su, X. Liu, and S. Hui, IEEE Transactions On Power Electronics **24**, 1115 (2009).
[29] J. Acero, C. Carretero, I. Lope, R. Alonso, O. Lucia, and J. Burdio, IEEE Transactions On Industrial Electronics **60**, 410 (2013).
[30] T. Reissman, J. Park, and E. Garcia, Active And Passive Electronic Components (2012).
[31] J. Burghartz and B. Rejaei, IEEE Transactions On Electron Devices **50**, 718 (2003).
[32] S. Mohan, M. del Mar Hershenson, S. Boyd, and T. Lee, IEEE Journal Of Solid-State Circuits **34**, 1419 (1999).